Journal of
Synchrotron Radiation

ISSN 0909-0495

Received 10 October 2007
Accepted 8 January 2008

Diffraction theory applied to X-ray imaging with clessidra prism array lenses

Liberato De Caro[a]* and Werner Jark[b]

[a]Istituto di Cristallografia, Consiglio Nazionale delle Ricerche (IC-CNR), via Amendola 122/O, I-70125 Bari, Italy, and [b]Sincrotrone Trieste ScpA, SS 14 km 163.5, I-34012 Basovizza (TS), Italy. E-mail: liberato.decaro@ic.cnr.it

Clessidra (hourglass) lenses, *i.e.* two large prisms each composed of smaller identical prisms or prism-like objects, can focus X-rays. As these lenses have a periodic structure perpendicular to the incident radiation, they will diffract the beam like a diffraction grating. Refraction in the prisms is responsible for blazing, *i.e.* for the concentration of the diffracted intensity into only a few diffraction peaks. It is found that the diffraction of coherent radiation in clessidra lenses needs to be treated in the Fresnel, or near-field, regime. Here, diffraction theory is applied appropriately to the clessidra structure in order to show that blazing in a perfect structure with partly curved prisms can indeed concentrate the diffracted intensity into only one peak. When the lens is entirely composed of identical perfect prisms, small secondary peaks are found. Nevertheless, the loss in intensity in the central peak will not lead to any significant widening of this peak. Clessidras with perfect prisms illuminated by full coherent X-ray radiation can then provide spatial resolutions, which are consistent with the increased aperture, and which are far below the height of the single small prisms.

Keywords: X-ray optics; kinoform lens; refraction; diffraction; spatial coherence.

1. Introduction

Only very recently have transmission lenses become a tool for focusing X-rays (Snigirev *et al.*, 1996). Today they are already commercially available objects, which can easily be procured and are thus in use in an increasing number of experiments.

The focal length of transmission lenses with two identically curved surfaces is given by (Born & Wolf, 1980)

$$f = R/[2(n-1)], \qquad (1)$$

where R is the radius of curvature of the lens surface on the optical axis (see Fig. 1*a*) and n is the refractive index of the lens material. In the X-ray range the refractive index is just slightly smaller than unity and is thus more conveniently written using the unit decrement δ as $n = 1 - \delta + i\beta$. The latter term is related to the beam attenuation. Then the focal length for X-rays becomes (Snigirev *et al.*, 1996)

$$f = -R/(2\delta), \qquad (2)$$

and the sign indicates that concave lens surfaces will focus an incident plane wave at the focal distance f downstream of the lens. In case the focal distance remains inconveniently long, one can shorten it in a stack of lenses for which

$$1/f = \sum_i 1/f_i,$$

or $f = -R/(2N\delta)$ if we use N identical lenses. The ideal lens shape is elliptical (Evans-Lutterodt *et al.*, 2003; Suzuki, 2004) but this is approximated quite well by a parabola (Lengeler *et al.*, 1999), which is the shape of the external lens surfaces in Figs. 1(*a*)–1(*c*). If we restrict the discussion to only one dimension, such a profile results in a Gaussian transmission function (Lengeler *et al.*, 1999; Cederström *et al.*, 2000), so obviously parabolic X-ray lenses have limited apertures. The latter vary with the square root of the focal length (Cederström *et al.*, 2000), so larger apertures are provided at longer

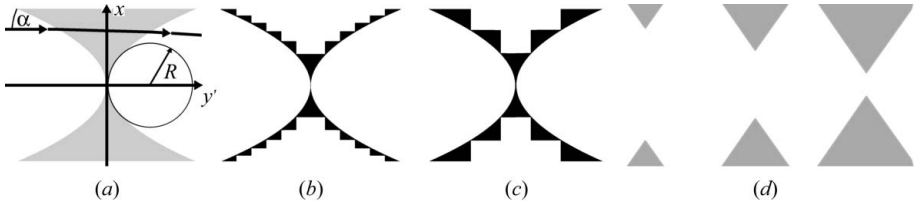

Figure 1
Cross section of transmission lenses for X-rays. (*a*) Bi-concave lens with parabolic surfaces. The lens in (*b*) is obtained from (*a*) by removing as many blocks of material as possible, which shifts the phase of the transmitted radiation by integer multiples of 2π. In the lens in (*c*) the same strategy is applied; however, now also the height of the blocks is kept constant. The cross section in (*d*) shows three prism pairs, obtained by inclining two dented plates with respect to each other. All objects are drawn to scale with the same focal length.

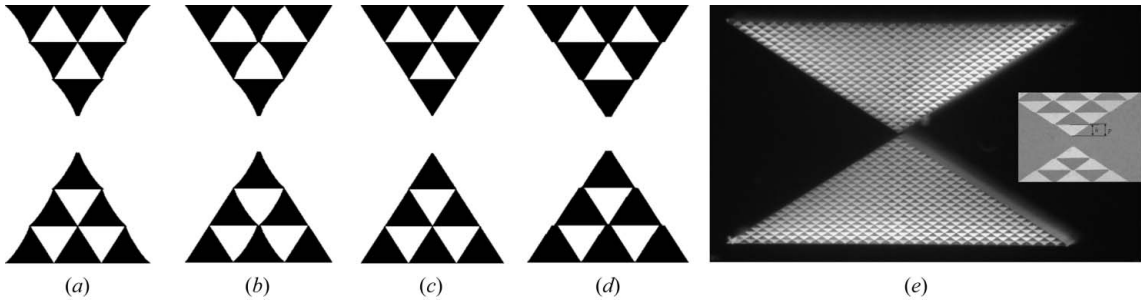

Figure 2
Lenses based on the material removal strategy presented in Fig. 1(*c*) obtained by re-arranging the remaining material. While in (*a*) and (*b*) the parabolic curvature is maintained in the outermost and in the innermost segment surfaces of any row, the lens in (*c*) is composed of perfect prisms. In the lens in (*d*) the lens from (*c*) was made more rigid by adding stiffening bars on the prism symmetry axis. (*e*) Micrograph of a Fresnel lens realised according to the scheme in (*b*). The inset shows details in the center of a lens of type (*d*). The prisms have a height of 25.67 μm and a width of 73.33 μm. The overall lens height is 1.5 mm and contains 58 prism rows.

focal length. An increase in numerical aperture, *i.e.* in the ratio between the lens half-aperture and focal length, which will permit smaller diffraction-limited resolution (Schroer *et al.*, 2003), requires shorter focal lengths to be used. Commercially available lenses have apertures that are smaller than 1 mm, and they are almost always arranged in stacks of identical lenses. With these parameters the use of such lenses is essentially limited to state-of-the-art synchrotron radiation sources, where even a small aperture at a large source distance can still intercept a large fraction of the available photon flux. Now the aperture can be increased if all optical inactive material is removed with the strategy invented by Fresnel to reduce the weight of lighthouse lenses. Optical inactive are blocks of material, which shift the phase of the passing radiation beam, compared with travel in air, by integer multiples of 2π. This removal can be optimized and two solutions have been tested up to now. In the first case, proposed by Suehiro *et al.* (1991) and first realised by Aristov *et al.* (2000), the amount of removed material is maximized for minimizing the absorption. This removal strategy is shown in Fig. 1(*b*) and results in segments of continuously changing height. Note that the remaining segments can also be arranged differently (Snigireva *et al.*, 2001; Nöhammer *et al.*, 2003; Evans-Lutterodt *et al.*, 2003; Nazmov *et al.*, 2004). The second solution was presented by Jark *et al.* (2004) and its functioning scheme is shown in Fig. 1(*c*). In this case the removal of the optically inactive blocks is made with blocks of constant height. This latter Fresnel lens was compacted to a highly regular structure (Jark *et al.*, 2004), with mostly identical prisms or prism-like segments arranged in rows, as shown in Fig. 2. In this structure all internal segments are connected to their neighbors at all three tips. This adds to the rigidity of the structure, which right now can only be produced as a one-dimensionally focusing object by deep X-ray lithography (Jark *et al.*, 2004; Pérennès *et al.*, 2005). The number of prisms per row increases with increasing distance from the optical axis, which gives the whole assembly an hourglass (in Italian: clessidra) shape. This clessidra lens is usually used either as a single lens or a lens tandem in orthogonal configuration for focusing in two dimensions (Jark *et al.*, 2004, 2006). With clessidras, one can keep the parabolic curvature either in the outermost or in the innermost segment sidewalls, as shown in Figs. 2(*a*) and 2(*b*), respectively. One of the principal questions is whether a clessidra with perfect and identical prisms will perform similarly to the other aberration-corrected clessidras in terms of obtainable spatial resolution. The natural solution for this concept is shown in Fig. 2(*c*). The object in Fig. 2(*d*) is a further modification, in which additional rigidity is obtained by adding a thin bar on the vertical axis of all prisms. The simple and highly regular shape of these latter objects facilitates very significantly the quality control and quality assurance in all critical steps of their production. This process involves an original mask, a replicated X-ray mask and the lens production by replicating the latter mask (Pérennès *et al.*, 2005). The micrograph in Fig. 2(*e*) shows a prototype lens of the type shown in Fig. 2(*b*). The inset in Fig. 2(*e*) shows the detail in the center of a perfect prism lens of the type shown in Fig. 2(*d*) (Pérennès *et al.*, 2005).

Originally the clessidra lens was derived by Jark *et al.* (2004) from the long-playing record lens presented by Cederström *et al.* (2000). The concept of this latter lens, also called the alligator lens owing to its appearance as an assembly of inclined dented plates (Dufresne *et al.*, 2001; Jark, 2004), is thus also shown in Fig. 1(*d*). This alligator lens approximates stepwise the required ideal parabolic profile (Cederström *et al.*, 2000). This can be seen in Fig. 3(*c*), where the amount of material to traverse is plotted with respect to the off-axis position.

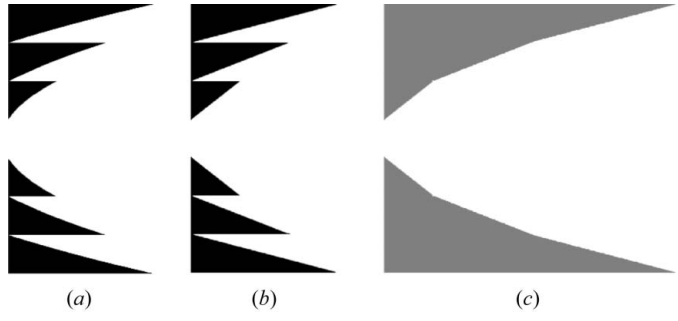

Figure 3
Total amount of material present in the clessidra lenses from Figs. 2(*a*) and 2(*c*) and in the Cederström lens from Fig. 1(*d*), depending on distance from the optical axis.

Figs. 3(*a*) and 3(*b*) show the amount of material in the different rows of aberration-corrected and perfect-prism clessidra lenses, respectively. At any off-axis distance the inclinations of the surface profiles are identical in Figs. 3(*b*) and 3(*c*). Compared with Fig. 3(*c*), in Fig. 3(*b*) a block of optically inactive material is removed, making Fig. 3(*b*) the Fresnel version of Fig. 3(*c*). Therefore, while the focal length of the Cederström lens from Fig. 1(*d*) is zoomable by changing the inclination angle, this is not possible with the clessidra lens, nor with the Fresnel lens in Fig. 1(*b*). These Fresnel lenses are to be used with sufficiently spatially coherent radiation at those photon energies for which the phase shift in the removed blocks is an integer multiple of 2π.

2. Theoretical considerations

2.1. Basic remarks

Up to now the functioning of these special X-ray Fresnel lenses has been discussed regarding them mostly as refractive objects (Jark *et al.*, 2004). In that case the focusing is immediately understood when it is recognized that the X-ray beam is refracted in a symmetric prism by an angle (Cederström *et al.*, 2000)

$$\Delta_{\rm ref} = -2\delta/\tan\alpha. \tag{3}$$

Here α is the angle of grazing incidence onto the prism sidewall and the exit angle is approximately identical to it. The sign indicates a refraction towards the prism tip. For prisms of height h the refractive focal length is then

$$f_{\rm ref} = \frac{h\tan\alpha}{2\delta}. \tag{4}$$

If we now compare the material distributions in Fig. 3 with a perfect parabolic profile, we see that clessidras as well as the alligator lens will introduce periodic disturbances in the transmitted wavefield in the direction perpendicular to trajectories of the incident beams. These disturbances are either only phase discontinuities (Fig. 3*a*) or only small distortions (Fig. 3*c*) or both (Fig. 3*b*). These field distortions are periodic and thus these lenses become diffracting objects, *i.e.* linear transmission gratings. Optimally the trajectory of one of the diffraction directions for a particular row should coincide with the trajectory of the rays refracted in this row. Then we should find an intense peak on the optical axis of the lens.

The diffractive focal length has already been derived by Jark *et al.* (2006) as

$$f_{\rm diff} = h^2/m\lambda. \tag{5}$$

Here m is the number of 2π phase shifts in the prism bases. The refractive and the diffractive focal length will obviously coincide for

$$\lambda = h\,2\delta/m\tan\alpha. \tag{6}$$

We see that for a proposed lens we need to accept a relative error in the operation wavelength, which is identical to the relative error in the knowledge of δ.

In a practical lens we would always illuminate coherently more then one prism row. From (5) we then see that the illuminated area A ($A > h$) fulfills for small m the condition $A^2 > \lambda q$, where q is the distance of the observation plane from the lens, *i.e.* a number similar to f. The indicated condition requests the diffraction in or close to the focal plane of a clessidra to be considered in the near-field or Fresnel regime (Born & Wolf, 1980). In this regime simple linear binary diffraction gratings will produce periodic line structures at the so-called Talbot distances (Talbot, 1836), which are given by

$$D_{{\rm Tal},k/l} = kh^2/l\lambda, \tag{7}$$

with both k and l being integers. Obviously the principal clessidra focal distance coincides with the Talbot distance for $k = 1$ and $l = m$. At these positions the period in the image would be h/l, *i.e.* an integer fraction $1/l = 1/m$ of the grating periodicity h. For $l > 1$ we would also speak of the fractional Talbot effect (Arrizón & Ojeda-Castaneda, 1994). As we are in the regime of near-field diffraction and as we deal with a rather small finite number of structures, we have to ask the question of how far the 'imperfections' in the structure can affect the lens performance with special concern on the achievable spatial resolution. Here we will thus treat theoretically the following problems. Will the periodic clessidra structure with curved prisms really focus like a lens with parabolic surfaces? Will clessidra with perfect prisms still focus identically, *i.e.* can the resolution be much smaller than the prism height? What happens if the lens is operated off the optimum photon energy? And what will happen if the prism tips have a finite size? The answers to the second and the last question are also very interesting for operation of the alligator lens (Shastri *et al.*, 2007).

Jark *et al.* (2006) have already discussed the fact that the focus broadening owing to chromatic aberrations in larger-aperture clessidras will eventually require their operation with a monochromator bandwidth below the intrinsic spectral resolution limit of standard Si(111) double-crystal monochromators. Instead the bandwidth requirement for sufficient longitudinal coherence is less severe (Jark *et al.*, 2006). Here we will assume a sufficiently monochromatic incident beam.

2.2. Detailed discussion of diffraction in clessidra lenses

As clessidras and alligator lenses are one-dimensionally focusing objects, we will treat the diffraction in only one dimension. The extension to two-dimensional focusing is then easily possible for all objects in which the transmission function is factorisable with respect to two orthogonal axes.

As we deal with an optical component for synchrotron radiation, we can assume its aperture to be significantly smaller than its distance p from the source and than its focal distance f. For the moment we will also assume that the overall object extension in beam direction is significantly smaller than its focal length and that the incident radiation is fully coherent. The beam will travel in the y direction and is focused in the x direction. $x = 0$ refers to the optical axis of the set-up. Then we can use the paraxial approximation for the Fresnel propaga-

tors, which allows us to calculate the complex field amplitude in the detector plane using the Fresnel–Kirchoff integral (Born & Wolf, 1980) in the form

$$A(x_q) = \frac{1}{i\lambda(pq)^{1/2}} \iint \mathrm{d}x_p \mathrm{d}x\, \Psi(x_p) \exp\left[i\pi(x - x_p)^2/p\lambda\right] \times \exp\left[i\pi(x_q - x)^2/q\lambda\right] P_{\mathrm{lens}}(x), \quad (8)$$

where $\Psi(x_p)$ is the complex amplitude emitted by the coherent source. The integration in $\mathrm{d}x_p$ is performed over the source linear dimension. The two exponential factors, *i.e.* the Fresnel propagators, describe the wavefield propagation in free space from the source to the front of the lens at distance p, and from the back of the lens to the detector at distance q. The last term in (8) is the lens propagator[1], which can be written as (Snigirev *et al.*, 1998; Kohn *et al.*, 2003)

$$P_{\mathrm{lens}}(x) = \exp[-i2\pi(\delta - i\beta)t(x)/\lambda], \quad (9)$$

where $t(x)$ is the lens transmission function. This expression for the lens propagator corresponds to a local approximation of the modification of the incident wavefield caused by the lens. At this point the latter is thus assumed to be a planar object. This is possible as long as the ratio of the lens extent in beam direction L to focal length (L/f) is much less than 10^{-1}. Otherwise the corrections discussed by Kohn *et al.* (2003) will have to be taken into account. In the latter case, clessidras will also have to be designed with curved rows in which the prism bases follow adiabatically the curved beam trajectories as discussed by Schroer & Lengeler (2005).

If we are at the optimum wavelength, ignore the absorption and assume incident plane waves, we can simplify the discussion significantly. We will introduce here the unitless off-axis distance $\bar{x} = x/h$; then the propagator of a parabolic profile lens is

$$P_{\mathrm{Para}}(\bar{x}) = \exp\left(-i\frac{2\pi}{\lambda}\,\delta\,\frac{h^2\bar{x}^2}{2f}\right). \quad (10)$$

Now in the jth row of a clessidra the parameter $\bar{x}$ varies from $j - 1/2$ to $j + 1/2$, and the difference in phase shift in a clessidra compared with a parabolic profile lens is periodic with constant amplitude, if we ignore phase shifts, which are modulus 2π. This periodic correction is shown in Fig. 4 for $m = 1$ (note that the amplitude increases linearly with m).

We can now very conveniently write the propagator of the clessidra profile in row j as

$$P_{\mathrm{Cles}}(j, \bar{x}) = P_{\mathrm{Para}}(\bar{x}) \exp\left[i2\pi m(\bar{x} - j)^2/2\right] \times \exp\left[i2\pi m\left(j^2 - |j|\right)/2\right], \quad (11)$$

with

$$m = b\delta/\lambda, \quad (12)$$

[1] Actually the lens propagator would be given by the phase factor given by equation (9) multiplied by a delta-function $\delta(x - x_{\mathrm{in}})$ with x_{in} on the front of the lens and x on the back of the lens. For the properties of the delta-function, integrating on the coordinate x_{in}, one would obtain the simplified phase factor of equation (9).

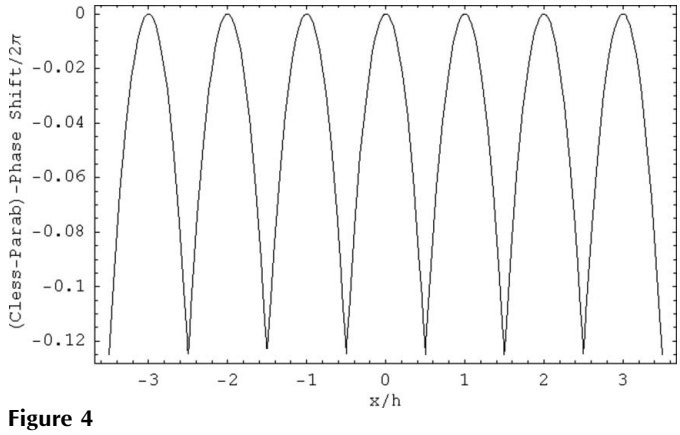

Figure 4
Difference in phase shift in a clessidra compared with a parabolic profile lens, modulo 2π, for $m = 1$.

where b is the prism base length. Equation (11) holds for the perfect prism lens of Fig. 2(*c*). The last phase factor of equation (11) is due to blocks of optically inactive material removed, which makes Fig. 3(*b*) the Fresnel version of Fig. 3(*c*). At the optimum wavelength (m integer) and neglecting absorption, this last phase factor can be neglected and clessidra and alligator lenses become equivalent. In the last part of this section we will discuss the cases $m \neq$ integer and $w > 0$, *i.e.* a clessidra lens as shown in Fig. 2(*d*) operated away from the optimum wavelength. If the whole number $N_{\mathrm{T}} = (2N + 1)$ of rows is sufficiently high one can expand the periodic part of the phase shift of equation (11) into a Fourier series obtaining

$$P_{\mathrm{Cles}}(\bar{x}) = P_{\mathrm{Para}}(\bar{x}) \sum_{j=-N}^{N} c_j \exp(-2\pi j i\bar{x}), \quad (13)$$

where the Fourier coefficients c_j are given by

$$c_j = \int_{-1/2}^{1/2} \exp\left(\pi i m\bar{x}^2\right) \exp(2\pi i j\bar{x})\, \mathrm{d}\bar{x} = \frac{(-1)^{1/4}\exp(-\pi i j^2/m)}{2m^{1/2}} \times \left\{\mathrm{Erf}\left[\frac{(-1)^{3/4}\pi^{1/2}(2j - m)}{2m^{1/2}}\right] - \mathrm{Erf}\left[\frac{(-1)^{3/4}\pi^{1/2}(2j + m)}{2m^{1/2}}\right]\right\}. \quad (14)$$

When we make the observation distance unitless, *i.e.* $a = q/f$, then the solutions for both profiles are given by equations (26) and (27) of Appendix *A*. Let us recall for the following discussion, where mostly only the clessidra lens is mentioned, that without absorption the clessidra lens with perfect prisms and the alligator lens are equivalent.

For $a = 1$, *i.e.* in the focal plane, the maxima of I_{Para} and I_{Cles} are ${N_{\mathrm{T}}}^2$ and ${N_{\mathrm{T}}}^2|c_o|^2$, respectively. Thus, the periodic phase-shift in (11) leads to a smaller maximum intensity of the clessidra with respect to the parabola, and to the presence of small secondary maxima for $x = \pm nh/m$, with n integer. For $m = 1$, since $|c_o|^2 = |\mathrm{Erf}[\pi^{1/2}(-1)^{3/4}/2]|^2 = 0.946$, the zero-order maximum is slightly smaller than ${N_{\mathrm{T}}}^2$, and only the two first-

order secondary maxima at $x = \pm h$ have a non-negligible intensity. These findings can be seen in Fig. 5(*a*), where we show a comparison of the profiles in the focus ($a = 1$) for a parabolic lens (dotted curve) and clessidra without prism curvature (continuous curve), for $N_T = 31$, $m = 1$, energy = 8 keV, $h = 25.67$ µm, $\delta = 4 \times 10^{-6}$ and $b = m\lambda/\delta$. In Fig. 5(*b*) the continuous and dashed curves show the difference between the profiles obtained for the clessidra with curved and with perfect prisms with respect to a parabola (see Appendix *A* for equations). As expected, the lacking intensity in the central peak, amounting to ∼5%, is divided equally onto the first secondary peaks at $\bar{x} = \pm 1$. We see that, as far as the obtainable spatial resolution is concerned, the decrease in the maximum intensity has almost no reduction effect on the width of the central peak in the full width at half-maximum (FWHM) sense. In fact, the peak width in a clessidra with perfect prisms is identical to the resolution obtainable with an absorptionless parabolic profile of the same aperture. Now in diffraction optics (Born & Wolf, 1980) the resolution is given by

$$d = c\lambda/2\mathrm{NA}. \tag{15}$$

Here, c is a numerical coefficient close to unity; NA is the numerical aperture, which is given by half of the lens aperture divided by the focal distance. Applying (5) one obtains NA = $0.5N_T h/f_{\mathrm{diff}} = 0.5N_T m\lambda/h$, and, therefore, $d = ch/mN_T$. The simulations obtained by equation (26) indicate that the FWHM width of the main peak for the clessidra lens is given by $0.88h/mN_T$. Here the coefficient $c = 0.88$ is characteristic of the particular profile of the diffracting object (Born & Wolf, 1980). Taking into account absorption, N_T should be substituted by the effective number of rows, which will then form the corresponding effective lens aperture. We see that in any case the spatial resolution d obtainable in clessidra lenses can be significantly smaller than the height of the perfect prisms. The same holds true for the alligator lens. It is interesting to see that in lenses with given N_T and h the resolution should improve for numbers $m > 1$. This is due to the reduction in focal length according to (5) for otherwise unchanged lens aperture. In this case the first secondary diffraction peaks are expected closer to the central peak at $x = \pm h/2$. We have to recognize that, *e.g.* for $m = 2$, the periodic correction to the phase shift in clessidras with perfect prisms compared with the ideal parabolic profile is now increased to twice the amount shown in Fig. 4. This more significant disturbance, which arrives at a quarter of 2π, now reduces the prefactor in equation (27) to $|c_o|^2 = 0.8$. Most of the missing intensity goes into the first-order peaks, but the second-order peaks are now also present. Now the principal peak is more significantly reduced in intensity. Nevertheless its FWHM width is almost as expected at about 50% of the width for $m = 1$. These aspects can be seen immediately in Fig. 5(*c*), in which the abscissa range is reduced by a factor of two, such that the peak width and the positions of the first-order peaks can be compared directly with Fig. 5(*a*) for $m = 1$.

In Fig. 6 we show a contour plot of I_{Cles} as a function of the unitless parameters $\bar{x}$ and a, for $N_T = 31$, photon energy = 8 keV, $h = 25.67$ µm, $\delta = 4 \times 10^{-6}$ and $b = m\lambda/\delta$, here with $m = 1$. We note that all waves exiting from the lens rows converge towards the focus at $a = 1$ and $\bar{x} = 0$. As already shown in Fig. 5(*a*), we find the first secondary maximum caused by the wavefield distortion in the perfect prisms at $a = 1$, $\bar{x} = 1$. The second-order peak at $a = 1$, $\bar{x} = 2$ is missing instead. But we also have to note that the regular line patterns are no longer found at fractional Talbot distances. They also do not show the expected periodicity.

In order to understand this point let us note that the pattern that one would obtain considering only the periodic phase shift component of equation (11) would be given by

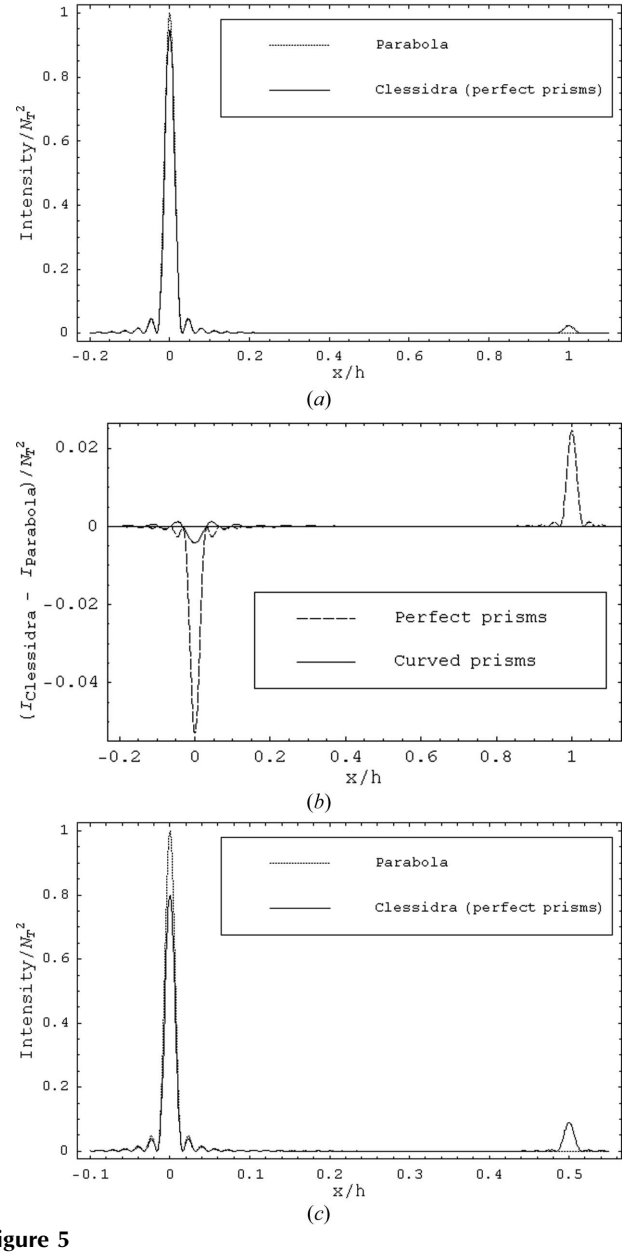

Figure 5
(*a*) Comparison of the intensity profiles in the focus ($a = 1$) for a parabolic lens (dotted curve) and clessidra without prism curvature (continuous curve), for $N_T = 31$, $m = 1$, energy = 8 keV, $h = 25.67$ µm, $\delta = 4 \times 10^{-6}$ and $b = m\lambda/\delta$. (*b*) Differences between the intensity profiles for a clessidra with curved (continuous curve) and with perfect (dashed curve) prisms with respect to the intensity profile for a parabola. (*c*) Same as in (*a*) but for $m = 2$.

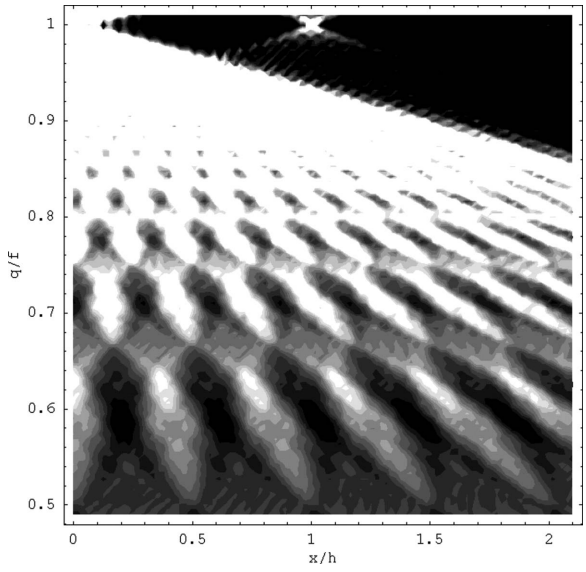

Figure 6
Contour plot of $I_{\rm Cles}$ as a function of $\bar{x}$ and a, for $N_{\rm T} = 31$, $m = 1$, energy = 8 keV, $h = 25.67$ µm, $\delta = 4 \times 10^{-6}$ and $b = m\lambda/\delta$.

$$A_{\rm periodic}(\bar{x}, a) = \frac{h}{(i\lambda q)^{1/2}} \int_{-\infty}^{\infty} \exp\left[\frac{i\pi(\bar{x} - \bar{x}')^2}{q\lambda/h^2}\right] P_{\rm Cles}(\bar{x}') / P_{\rm Para}(\bar{x}')\, {\rm d}\bar{x}' = -\sum_j c_j \exp\left(-i\pi j^2 a/m\right) \exp(-i2\pi j\bar{x}). \quad (16)$$

The above pattern would give periodic repetitions of the diffraction grating just in correspondence of rational a values predicted by (7), where $\exp(-i\pi j^2 a/m) = \exp(-i2\pi l)$ with l integer, but the period of the repetitions would always be h for any a. Note that in this case without the parabolic profile the focusing effect is absent. On the other hand, when the phase shift is described by (11), we obtain a more complex intensity pattern [equation (26)] presenting features of varying period $h(a) = |1 - a|h$ in correspondence with particular a ranges which favour the constructive interference of the row waves. These intervals of constructive interference are separated by regions of destructive interference (see Fig. 6).

In the case of a periodic clessidra structure with curved prisms characterized by parabolic profiles we can write the propagator in the row j (for $w = 0$) as follows,

$$P_{\rm Cles-cur}(j, \bar{x}) = P_{\rm Para}(\bar{x}) \times \exp\left\{i2\pi\left[m\frac{(\bar{x} - j)^2}{2} - m_j\frac{(\bar{x} - j - \bar{x}_c)^2}{2}\right]\right\} \times \exp\left(i2\pi m\,\frac{j^2 - |j|}{2}\right). \quad (17)$$

Here the parameter m_j is related to the curvature of the lateral sides of the prism in the jth row, and $\bar{x}_c = x_c/h$ defines the symmetry centre of the prism parabolic profiles. Since in the row $j = 0$, $m_j = 0$ (there is no prism) and for any other $j \neq 0$ one has $m_j \neq 0$, the phase shift has a periodic term only in the two half lenses, but not in the central gap. The lack of periodicity on the whole lens means it is impossible to use the Fourier series expansion [equation (13)]. Nevertheless, since the phase shift [equation (17)] depends on the row index j, inserting (17) into (25), after integration from $j - 1/2$ to $j + 1/2$, the final result for the intensity would always be obtained by a sum over all rows, and is reported in Appendix A [see equation (28)]. For $j \neq 0$, $m_j = m$ and $x_c = 0$, the parabolic profile propagator $P_{\rm Para}$ would be perfectly reproduced everywhere except in the central gap.

The resultant difference between the simulations by use of equation (28) for the clessidra, with the parameters of Fig. 5 and with curved prisms, and the perfect parabolic lens is shown in Fig. 5(b). Now the secondary maximum at $x = h$ is missing in this aberration-corrected clessidra lens, while the intensity in the central peak is decreasing by an insignificant 0.5%. This small difference is caused by the absence of a focusing effect in the central gap. At all other unitless observation distances $a = q/f$ the intensity patterns from both profiles essentially coincide with a complete absence of Talbot-like features. However, when $\bar{x}_c \neq 0$, even if $m_j = m$ for any $j \neq 0$, Talbot-like features reappear owing to the displaced periodic phase shift in each lens half. For $\bar{x}_c = 1/2$, a saw-tooth phase-shift function would be obtained instead of that shown in Fig. 4. For any other $\bar{x}_c$, the shape of the periodic function would be a more complex quadratic function.

Finally, we generalize our model to take into account detuning effects owing to erroneous photon energy settings and to additional tips w in any prism. For prisms with linear lateral sides, by summing all tips in the jth row we can write the lens propagator as follows,

$$P_{{\rm Cles}-w}(j, \bar{x}) = \exp\left(-i\pi m\bar{x}^2\right) \exp\left[i\pi m(\bar{x} - j)^2\right] \times \exp\left[i\pi m\left(j^2 - |j|\right)\right] \times \exp\left\{-i\pi m\bar{w}[|j| + 2j(j - \bar{x})]\right\}. \quad (18)$$

Here $m = m_0 + \Delta m$, where m_0 is the integer value of 2π phase-shift that would be obtained for the correct energy setting; the real part of Δm is related to the energy detuning; its imaginary part is related to the absorption by equation (9); $\bar{w} = w/b$ is the dimensionless tip size, normalized with the prism base b. The four-phase terms of (18) are, respectively, due to: the parabolic profile; the clessidra profile correction; blocks of optically inactive material removed; finite size of the tips. Moreover, in order to partially compensate the last phase shift of (18), one could argue to do this by enlarging the central gap. If we denote by $2\bar{s}$ ($\bar{s} = s/h$) the unitless increment of the central gap, defining $a = q/(h^2/m_0\lambda)$, from (25) and (18) one has

$$I_{{\rm Cles}-w}(\bar{x}, a, \bar{w}, \bar{s}, \Delta m) = \left|A_{\rm gap}(\bar{x}, a) + A_{\rm left}(\bar{x}, a) + A_{\rm right}(\bar{x}, a)\right|^2, \quad (19)$$

where the amplitudes of the central gap, the left and right halves of the clessidra lens are reported in Appendix A. In Fig. 7(a) we show the intensity on the optical axis given by a clessidra lens for $N_{\rm T} = 31$, $m = 1$, energy = 8 keV, $h = 25.67$ µm, $\delta = 4 \times 10^{-6}$, as a function of a: ideal case (continuous curve); energy detuning by 3% (dashed curve); introduction of tips with size w, which amount to 3% of b (short-dashed curve);

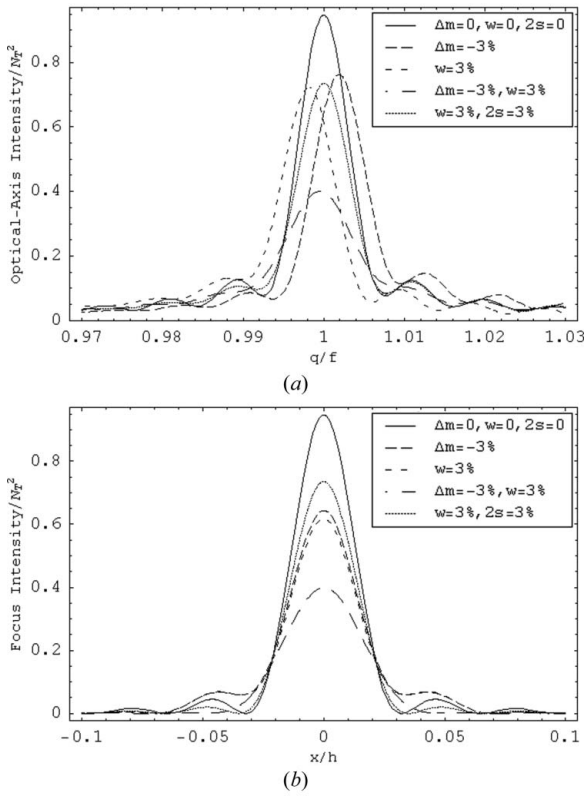

Figure 7
(*a*) Intensity on the optical axis calculated for a clessidra lens for $N_T = 31$, $m = 1$, energy = 8 keV, $h = 25.67$ µm, $\delta = 4 \times 10^{-6}$, $m_0 = 1$ and $b = m\lambda/\delta$, as a function of $a = q/f$. Ideal case, continuous curve; energy detuning, dashed curve; tips of size w, short-dashed curve; compensating w with detuning, long-dashed curve; compensating w with a larger central gap, dotted curve. (*b*) Intensity at the focus distance calculated for a clessidra lens as a function of x/h. The parameters are the same as in (*a*).

compensation of the effect of a finite w by detuning (long-dashed curve); compensation of the effect of a finite w with a larger central gap (dotted curve). In Fig. 7(*b*) we show the intensity at the focus distance as a function of x/h for the same cases as in Fig. 7(*a*). The plotted curves have been obtained using equations (19), (29) and (30). Note that both detuning and the presence of tips reduce the constructive interference and modify the focus distance. The detuning is not an efficient means of compensating the effect of tips, as it deteriorates the lens performance in terms of flux and spatial resolution. The effect of the tips is then better compensated for by adjusting the central gap without detuning the photon energy. Note that no correction will be needed if we use only one half of the clessidra structure. The simulations indicate that if we express the detuning as Δm such that $m \neq$ integer, the permitted detuning, also in a half lens, is proportional to $1/m_0N_T$. For the present numerical example with $N_T = 31$ and $m_0 = 1$, only a detuning or a photon energy setting error corresponding to $\Delta m < 0.02$ can be tolerated. Moreover, simulations with unitless variables indicate that the following condition between the geometrical prism parameters has to be satisfied: $\bar{w} \simeq 2\bar{s}$, when $\bar{w}$ is of the order of a few percent. In terms of absolute numbers, for w and s one has $wh \simeq 2bs$. For $\bar{w}$ values exceeding a few percent, the optimal central gap width can only be obtained from detailed simulation. If we return to perfect prism clessidras without tips, the results show that this concept has the potential to be a further alternative approach for obtaining particularly small focii. As shown by Schroer & Lengeler (2005), this will need curved prism rows. On the other hand, the prisms can remain rather large compared with the desired focus size. Given a lower limit for the feasible feature size, this will permit more prism rows than in a normal kinoform lens. And the correspondingly larger aperture will allow a desired focus size to be achieved at a larger focal length and thus farther from the lens.

3. Discussion of experimental data

This present theoretical study was made for completely spatially coherent illumination of the clessidra lens structure. On the other hand, our state-of-the-art clessidra lenses have rather large apertures in the mm range. Thus we succeeded to operate them only with partially spatially coherent radiation far above the diffraction-limited spatial resolution, as given by their effective apertures. So the presented conclusions for the obtainable resolution cannot be substantiated yet with experimental data. Nevertheless even in only partially spatially coherent illumination of clessidras could we already verify that very little intensity is diffracted into higher orders, when the lens is operated at the optimum photon energy. We take as an example a lens with perfect prisms made of PMMA with $h = 25.67$ µm and with $m = 2$ for a photon energy of about 8 keV. The performance of this lens in terms of refraction efficiency has already been discussed earlier by Jark *et al.* (2006, 2007). Now the optimum operation energy was found to be 7.9 keV and the test covered $N_T = 20$ and $N_T = 40$. Consistent with the expectation for clessidras with $m = 2$, the intensity diffracted into each of the first higher-order peaks amounted to less than 15% of the intensity in the central peak, and it was significantly smaller in all other higher-orders peaks. In agreement with Fig. 7, a small detuning of the photon energy made the higher-order peaks grow rapidly in intensity. After a detuning of only 2.5% the intensity in the first higher order already dominated over the intensity in the central peak.

The case of partially spatially coherent illumination is more likely to be found when operating kinoform lenses, which can have particularly large apertures (Jark *et al.*, 2006). We will thus address this problem in our future work and discuss the available experimental data in the framework of such a more appropriate study (De Caro & Jark, 2008).

4. Conclusions

We see that a clessidra with curved prisms performs almost identically to the parabolic profile as far as the achievable diffraction-limited spatial resolution is concerned. Even if the lens is composed throughout of identical non-curved prisms, under suitable experimental conditions the resolution remains unaffected; however, a small amount of intensity is diffracted into a first side peak. This result is also applicable to the alligator lens. Then for the clessidra and the alligator lens the

obtainable spatial resolution does not depend on the size of the prisms (or on the step height), but only on the total aperture. In other words, if a certain numerical aperture NA in (15) can be realised with different combinations of prism height h, N_T and m, then, as long as the apertures of these lenses are always spatially coherently illuminated, it is not an advantage for the obtainable spatial resolution to use the smallest possible prism height. This latter prism height reduction was pursued by Cederström *et al.* (2005). They kept the columns of prisms with equal height independent and allowed for steps between adjacent columns, which were smaller than the prism height.

Prism tips do not deteriorate the focus size as long as one can adjust the central gap in the lens accordingly. However, one will unavoidably lose some intensity in the central peak. This result is particularly interesting also for the operation of alligator lenses, for which it was not recognized before. In fact, also in these lenses the presence of flat tips of constant width will not deteriorate the resolution, as long as we can appropriately adjust the separation between the two jaws. In these lenses the photon energy tunibility can be maintained. Some photon energy tuning is also possible in clessidras, though only in a very small range, if we do not want to lose spatial resolution. The relative tuning interval depends reciprocally on the number of the present prism rows.

The presented equations provide the tools that allow us to simulate the lens operation as a function of the physical parameters involved in the diffraction process, such that suitable experimental conditions for best lens performances can be predicted. The case of partially spatially coherent illumination will be easily encountered with large aperture kinoform lenses and this problem will thus be addressed in a future work.

APPENDIX *A*

If we take a polynomial of second order for the lens transmission function, *i.e.* a parabolic profile with or without an overlayed linear profile, we can find a general analytical solution of equation (8). In fact, for

$$t_j(x) = a_{0,j} + a_{1,j}x + a_{2,j}x^2, \tag{20}$$

and for a coherent Gaussian source with a root mean square σ_s, we obtain

$$\begin{aligned} A(x_q) = i\sqrt{\frac{1}{q(\lambda p - 2\pi\sigma_s^2 i)}} \\ \times \sum_{j=-N}^{N} \exp\left[-i\frac{2\pi}{\lambda}(\delta - i\beta)a_{0,j}\right] \exp\left[i\pi\frac{UW_j - V_j^2}{\lambda W_j}\right] \\ \times \left\{\frac{\mathrm{Erf}\left[\frac{(-1)^{3/4}\sqrt{\pi}(W_j x_j - V_j)}{\sqrt{\lambda W_j}}\right] - \mathrm{Erf}\left[\frac{(-1)^{3/4}\sqrt{\pi}(W_j x_{j+1} - V_j)}{\sqrt{\lambda W_j}}\right]}{2\sqrt{W_j}}\right\} \end{aligned} \tag{21}$$

where the standard function Erf is defined as follows,

$$\mathrm{Erf}[z] = \frac{2}{\sqrt{\pi}}\int_0^z \exp(-y^2)\,\mathrm{d}y, \tag{22}$$

and

$$\begin{aligned} U &= \frac{x_q^2}{q}, \\ V_j &= \frac{x_q}{q} + (\delta - i\beta)a_{1,j}, \\ W_j &= \frac{1}{p - (2\pi\sigma_s^2/\lambda)i} + \frac{1}{q} - 2(\delta - i\beta)a_{2,j}. \end{aligned} \tag{23}$$

Here the index j runs over all the $2N + 1$ rows constituting the lens. The intensity of the beam after the lens in every point (x_q, q) is obtained from the square modulus of equation (21). This solution is also valid in the specific case of the clessidra lens. In fact, in this case the material distribution function for perfect prisms in row j is given by a linear transmission function,

$$t_j(x) = a_{0,j} + a_{1,j}x = \begin{cases} |j|w + j\frac{b-w}{h}(x - x_{j-1}) & \text{if} \quad x \geq 0, \\ |j|b + j\frac{b-w}{h}(x - x_{j-1}) & \text{if} \quad x < 0, \end{cases} \tag{24}$$

where $x_j = h/2 + jh$, with $j \in \{-N, -N + 1, \ldots, -2, -1, 0, 1, 2, \ldots, N - 1, N\}$; h, b and w are the prism height, the width of the prism at its base and the width of an eventually finite-size tip, respectively.

For an incident plane wave the above equations can be simplified. The complex field amplitude in the detector plane placed at a distance q from a lens with propagator P_{lens} is given by

$$A(x) = \frac{1}{\sqrt{i\lambda q}}\int_{-h/2+Nh}^{h/2+Nh} \exp\left[\frac{i\pi(x - x')^2}{q\lambda}\right] P_{\mathrm{lens}}(x')\,\mathrm{d}x'. \tag{25}$$

When $w = 0$, neglecting absorption, at the optimum wavelength (m integer), the propagator of either a clessidra or a parabolic lens can be defined as in (11). After a Fourier series expansion of the periodic part of the lens propagator [equations (13) and (14)] by equation (25), one has

$$\begin{aligned} I_{\mathrm{Cles}}(\bar{x}, a) = \left| \sum_{j=-N}^{N} \frac{c_j \exp\{-i\pi[aj^2 + m\bar{x}(m\bar{x} + 2j)]/m(a-1)\}}{2i\sqrt{m(a-1)}} \right. \\ \times \left\{ \mathrm{Erf}\left[k\left(\frac{aj}{m} + (1-a)\frac{N_T}{2} + \bar{x}\right)\right] \right. \\ \left. \left. - \mathrm{Erf}\left[k\left(\frac{aj}{m} + (a-1)\frac{N_T}{2} + \bar{x}\right)\right]\right\}\right|^2, \end{aligned} \tag{26}$$

$$I_{\rm Para}(\bar{x},a)=\left|\frac{\exp\left(-\frac{i\pi m\bar{x}^2}{a-1}\right)}{2i\sqrt{m(a-1)}}\left(\mathrm{Erf}\left\{k\left[(1-a)\frac{N_T}{2}+\bar{x}\right]\right\}-\mathrm{Erf}\left[k\left((a-1)\frac{N_T}{2}+\bar{x}\right)\right]\right)\right|^2, \tag{27}$$

where Erf(...) is the Erf-function defined in (22); $k=-[im\pi/(a^2-a)]^{1/2}$; c_j are the Fourier series expansion coefficients.

In the case of the periodic clessidra structure with curved prisms characterized by parabolic profiles we can write the lens propagator in the row j (for $w=0$) as given in (17). Thus, starting from (17), the integration from $j-1/2$ to $j+1/2$ and the summation over all rows lead to

$$I_{\rm Cles-cur}(\bar{x},a)=\left|\sum_{j=-N}^{N}\frac{\exp\left[i\pi m(j^2-|j|)\right]\exp\left[-\frac{i\pi\left[m(j-\bar{x})^2-m_j\left(j^2+(1+a)\bar{x}_c^2+2j(\bar{x}-\bar{x}_c)-2\bar{x}\bar{x}_c+\bar{x}^2\right)\right]}{1+a\left(1-m_j/m\right)}\right]}{2\sqrt{m+a\left(m-m_j\right)}}\right.$$
$$\times\left\{\mathrm{Erf}\left[\frac{i\sqrt{i\pi}\left(\frac{m_j}{m}(1+2\bar{x}_c)-1-a+2j-2\bar{x}\right)}{2\sqrt{1/a+\left(1-m_j/m\right)}}\right]\right.$$
$$\left.\left.-\mathrm{Erf}\left[\frac{i\sqrt{i\pi}\left(\frac{m_j}{m}(2\bar{x}_c-1)+1+a+2j-2\bar{x}\right)}{2\sqrt{1/a+\left(1-m_j/m\right)}}\right]\right\}\right|^2, \tag{28}$$

where the prism curvature parameters m_j and x_c are defined in the main text.

When $w\neq 0$, $m\neq$ integer, and the central gap is larger than h, one has to generalize the lens propagator as in equation (18), and integrate the two halves of the clessidra lens separately. From (18) and (25) it follows that the amplitude of the central gap is given by

$$A_{\rm gap}(\bar{x},a)=\frac{1}{2\sqrt{m_0}}\left\{\mathrm{Erf}\left[\frac{i\sqrt{im_0\pi}(\bar{x}-\bar{s}-1/2)}{\sqrt{a}}\right]-\mathrm{Erf}\left[\frac{i\sqrt{im_0\pi}(\bar{x}+\bar{s}+1/2)}{\sqrt{a}}\right]\right\}, \tag{29}$$

where $2\bar{s}=2s/h$ is the unitless increment of the central gap. The amplitude of the left-half lens is given by

$$A_{\rm left}(\bar{x},a)=\frac{1}{2\sqrt{m_0}}\sum_{j=-N}^{-1}\exp\left\{i\pi m\left[j^2(1-2\bar{w})-|j|\right](1+\bar{w})\right\}$$
$$\times\exp\left(-\frac{i\pi jm\left\{amj(\bar{w}-1)^2-m_0[j+2(\bar{x}+\bar{s})(\bar{w}-1)]\right\}}{m_0}\right)$$
$$\times\left\{\mathrm{Erf}\left[\frac{i\sqrt{i\pi}[2a\Delta mj(\bar{w}-1)]+m_0[-1+2j(1+a\bar{w}-a)-2(\bar{x}+\bar{s})]}{2\sqrt{am_0}}\right]\right.$$
$$\left.-\mathrm{Erf}\left[\frac{i\sqrt{i\pi}[2a\Delta mj(\bar{w}-1)]+m_0[1+2j(1+a\bar{w}-a)-2(\bar{x}+\bar{s})]}{2\sqrt{am_0}}\right]\right\}. \tag{30}$$

The amplitude of the right-half lens can be obtained by equation (30), changing $\bar{s}$ to $-\bar{s}$ and performing the summation from 1 to N.

References

Aristov, V., Grigoriev, M., Kuznetsov, S., Shabelnikov, L., Yunkin, V., Weitkamp, T., Rau, C., Snigireva, I., Snigirev, A., Hoffmann, M. & Voges, E. (2000). *Appl. Phys. Lett.* **77**, 4058–4060.

Arrizón, V. & Ojeda-Castaneda, J. (1994). *Appl. Opt.* **33**, 5925–5931.

Born, M. & Wolf, E. (1980). *Principle of Optics*, 6th ed. New York: Pergamon.

Cederström, B., Cahn, R. N., Danielsson, M., Lundqvist, M. & Nygren, D. R. (2000). *Nature (London)*, **404**, 951.

Cederström, B., Ribbing, C. & Lundqvist, M. (2005). *J. Synchrotron Rad.* **12**, 340–344.

De Caro, L. & Jark, W. (2008). In preparation.

Dufresne, E. M., Arms, D. A., Clarke, R., Pereira, N. R. & Dierker, S. B. (2001). *Appl. Phys. Lett.* **79**, 4085–4087.

Evans-Lutterodt, K., Ablett, J. M., Stein, A., Kao, C.-C., Tennant, D. M., Klemens, F., Taylor, A., Jacobsen, C., Gammel, P. L., Huggins, H., Ustin, S., Bogart, G. & Ocola, L. (2003). *Opt. Express*, **11**, 919–926.

Jark, W. (2004). *X-ray Spectrom.* **33**, 455–461.

Jark, W., Pérennès, F. & Matteucci, M. (2006). *J. Synchrotron Rad.* **13**, 239–252.

Jark, W., Pérennès, F., Matteucci, M., Mancini, L., Menk, R. H. & Rigon, L. (2007). *AIP Conf. Proc.* **879**, 796–799.

Jark, W., Pérennès, F., Matteucci, M., Mancini, L., Montanari, F., Rigon, L., Tromba, G., Somogyi, A., Tucoulou, R. & Bohic, S. (2004). *J. Synchrotron Rad.* **11**, 248–253.

Kohn, V., Snigireva, I. & Snigirev, A. (2003). *Opt. Commun.* **216**, 247–260.

Lengeler, B., Schroer, C., Tümmler, J., Benner, B., Richwin, M., Snigirev, A., Snigireva, I. & Drakopoulos, M. (1999). *J. Synchrotron Rad.* **6**, 1153–1167.

Nazmov, V., Shabel'nikov, L., Pantenburg, F.-J., Mohr, J., Reznikova, E., Snigirev, A., Snigireva, I., Kouznetsov, S. & DiMichiel, M. (2004). *Nucl. Instrum. Methods*, B**217**, 409–416.

Nöhammer, B., Hoszowska, J., Freund, A. K. & David, C. (2003). *J. Synchrotron Rad.* **10**, 168–171.

Pérennès, F., Matteucci, M., Jark, W. & Marmiroli, B. (2005). *Microelectron. Eng.* **78–79**, 79–87.

Shastri, S. D., Almer, J., Ribbing, C. & Cederström, B. (2007). *J. Synchrotron Rad.* **14**, 204–211.

Schroer, C. G. *et al.* (2003). *Appl. Phys. Lett.* **82**, 1485–1487.

Schroer, C. G. & Lengeler, B. (2005). *Phys. Rev. Lett.* **94**, 054802.

Snigirev, A., Kohn, V., Snigireva, I. & Lengeler, B. (1996). *Nature (London)*, **384**, 49–51.

Snigirev, A., Kohn, V., Snigireva, I., Souvorov, A. & Lengeler, B. (1998). *Appl. Opt.* **37**, 653–660.

Snigireva, I., Snigirev, A., Rau, C., Weitkamp, T., Aristov, V., Grigoriev, M., Kuznetsov, S., Shabelnikov, L., Yunkin, V., Hoffmann, M. & Voges, E. (2001). *Nucl. Instrum. Methods*, A**467**, 982–985.

Suehiro, S., Miyaji, H. & Hayashi, H. (1991). *Nature (London)*, **352**, 385–386.

Suzuki, Y. (2004). *Jpn. J. Appl. Phys.* **43**, 7311–7314.

Talbot, H. F. (1836). *Philos. Mag.* **9**, 401–407.